The Effect of Rotor Design on the Fluid Dynamics of Helicopter Brownout

Catriona Phillips
Postgraduate Research Assistant

Hyo Won Kim
Postdoctoral Research Assistant

Richard E. Brown*
Mechan Chair of Engineering

Rotorcraft Aeromechanics Laboratory
Department of Aerospace Engineering
University of Glasgow
Glasgow G12 8QQ
United Kingdom

Abstract

Helicopters operating close to the ground in dusty environments tend to generate large clouds of dust in the surrounding air. These clouds can obscure the pilot's view of the ground and lead to a dangerous condition known as brownout. Given the intimate relationship between the induced flow field around the rotor and the process through which the particulate matter becomes airborne and is subsequently transported, it has been speculated that the design of its rotor may influence the shape and size of the dust clouds that are produced by any particular type of helicopter. This paper presents a study of the influence of two key geometric properties of the rotor on the development of these dust clouds. A particle transport model is coupled to Brown's Vorticity Transport Model to represent the dynamics of the particulate-air system surrounding a generic helicopter rotor under various flight conditions. The number of blades on the rotor is altered, whilst keeping the solidity constant, thus altering the distribution of vorticity that is released onto the ground. In addition, the twist of the blades is varied in order to investigate the effect of the resultant changes in the distribution of induced downwash on the evolution of the dust cloud. The study suggests that, in general, the larger the number of blades, and the higher the blade twist, the less dense the dust clouds that are produced under brownout conditions. It appears thus that the characteristics of the dust clouds are indeed sensitive to the geometry of the rotor and hence that careful aerodynamic design may allow the severity of brownout to be ameliorated.

Nomenclature

C_T	rotor thrust, scaled by $\rho A(\Omega R)^2$
d	particle diameter
g	acceleration due to gravity
N_b	number of blades
R	rotor radius
S_p	source of particulates
S_ω	source of vorticity
θ_{tw}	total blade twist
μ	advance ratio
$\mu^\star$	thrust-normalised advance ratio, $\frac{\mu}{\sqrt{C_T/2}}$
ν	fluid viscosity
ν_p	particle diffusion constant
ρ	air density
ρ_p	local density of particulates in air
ρ_s	material density of particles
υ	velocity
υ_b	local on-blade velocity
υ_g	fallout velocity due to gravity
υ_t	threshold velocity
ω	vorticity
ω_b	bound vorticity

* Corresponding author; e-mail: rbrown@aero.gla.ac.uk

Presented at the 35th European Rotorcraft Forum, Hamburg, Germany, September 22-25, 2009.

Introduction

Whilst operating in desert or dusty conditions, particularly when flying close to the ground at low forward speeds, helicopters may suffer from a potentially dangerous condition known as brownout. During the onset of brownout, the wakes of the rotors entrain large clouds of dust into the air surrounding the helicopter causing the pilot to lose situational awareness. Understanding the aerodynamics associated with flight in ground effect may lead to a better understanding of the physical processes behind the formation of the dust cloud and may eventually allow sufficient insight

for the effects of brownout on helicopter operations to be ameliorated by passive aerodynamic design.

Computational modelling of the transport of particles within the flow field surrounding a helicopter can be conducted using two different methods. The first method, applied in the particle-fixed Lagrangian frame of reference, tracks the trajectories of a number of individual particles as they move through the flow field [1,2]. The properties of the overall dust field are then inferred from the behaviour of these particles. Although this method is fairly easily implemented it can become computationally expensive since a very large number of particles must be modelled if the variation in density of the dust within the flow field is to be estimated reliably. Most CFD-type methods for simulating the rotor flow itself are based in the helicopter- or ground-fixed Eulerian frame of reference, however. The transport of particles through the flow surrounding the helicopter can also be modelled in this frame of reference if the evolution of the dust density distribution is calculated using suitable transport equations. This method has been used by Ryerson *et al.* [3] and Haehnel *et al.* [4] and is also the approach that has been adopted in the present study.

Implementation of a particle entrainment and transport model into Brown's Vorticity Transport Model [5, 6] has allowed the onset and development of the dust clouds associated with helicopter brownout to be simulated. The similarity in mathematical form between the Eulerian particle transport equations and the vorticity transport equations results in a particularly efficient computational model for the brownout problem, as described in more detail by Phillips and Brown [7].

It is important to remark, however, that the best approach to modelling the initial entrainment of dust from the ground plane into the air in the helicopter context is still open to question. To date, published work investigating particle entrainment and the formation of dust clouds in the context of helicopter operations has been limited. For this reason, most models that are presently used to capture the entrainment of particles into the rotor flow have borrowed various semi-empirical elements from the field of riverine or aeolian sedimentology. Although the results obtained using this approach are very encouraging, further work is needed to clarify whether these semi-empirical models are fully applicable in the helicopter context. Nevertheless, recent experimental investigations [8,9] that have examined the entrainment of particles into the wakes of model rotors have revealed, at least qualitatively, very similar behaviour to that obtained using the numerical approach that has been adopted for the present study.

Anecdotal evidence from their operators and manufacturers suggests that different types of helicopters have very different brownout characteristics. It is thus thought that some of the geometric characteristics of its rotor might play an important role in determining the size and density of the dust clouds that are produced by any particular type of helicopter. In the present paper, the Vorticity Transport Model (VTM), coupled to an Eulerian transport model for the particulates in the flow, is used to investigate the extent to which two of these geometric characteristics, namely the number of blades and their twist, affect the size and shape of the dust clouds that develop around a helicopter rotor during hover and in forward flight at low altitude above a dusty surface.

Vorticity and Particle Transport Models

Brown's Vorticity Transport Model [5] has been extended to allow the transport of particles within the airflow surrounding the helicopter to be simulated. The VTM is a finite volume based method which calculates the evolution of the flow field surrounding a helicopter by advancing the solution to the vorticity-velocity form of the unsteady, incompressible Navier-Stokes equation

$$\frac{\partial}{\partial t}\omega + \upsilon \cdot \nabla\omega - \omega \cdot \nabla\upsilon = S_\omega + \nu\nabla^2\omega \qquad (1)$$

on a structured computational mesh. The velocity, υ, is related to the vorticity, ω, by the differential form of the Biot-Savart relationship, $\nabla^2\upsilon = -\nabla\times\omega$. The shed and trailed vorticity arising from the lifting surfaces immersed within the flow is introduced through the vorticity source term S_ω which can be written as

$$S_\omega = -\frac{d}{dt}\omega_b + \upsilon_b\nabla \cdot \omega_b \qquad (2)$$

where ω_b is the bound vorticity associated with each lifting surface of the helicopter.

The dynamics of a large number of particulates within an Eulerian frame of reference is governed by transport equations that can be derived from Newton's second law using classical statistical mechanics [7]. The transport equation for fine, suspended sediment can be written as

$$\frac{\partial}{\partial t}\rho_p + (\upsilon + \upsilon_g) \cdot \nabla\rho_p = S_p + \nu_p\nabla^2\rho_p \qquad (3)$$

where the source of particulates, S_p, represents the entrainment of particles from the ground plane into the flow field. Once in the flow, the effect of gravity on the dynamics of the particles is captured through the fallout velocity term υ_g. Although not used for the simulations presented in this paper, other terms can be included on the right hand side of the equation to model more accurately the spin-out of particles from vortex cores and also the scattering of particles as a result of collisions.

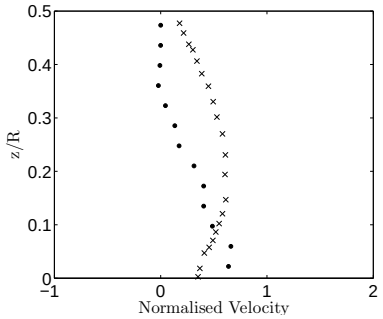

(a) $h/R = 0.5$

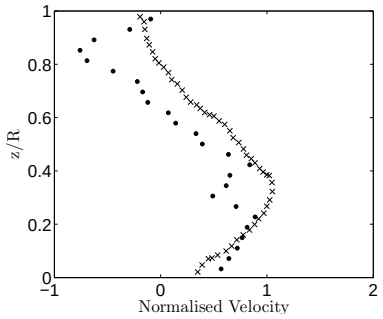

(b) $h/R = 1.0$

Figure 1: Profile of radial velocity at $r/R = 0.8$. (Crosses correspond to experimental data and dots to VTM predictions.)

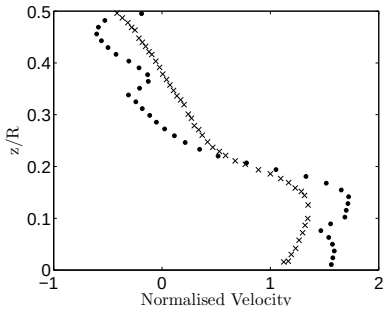

(a) $h/R = 0.5$

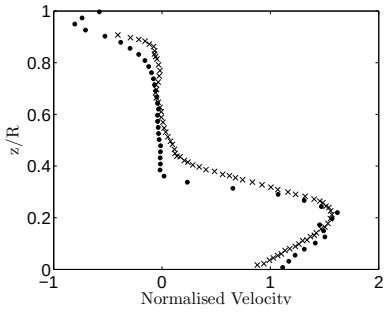

(b) $h/R = 1.0$

Figure 2: Profile of radial velocity at $r/R = 1.0$. (Crosses correspond to experimental data and dots to VTM predictions.)

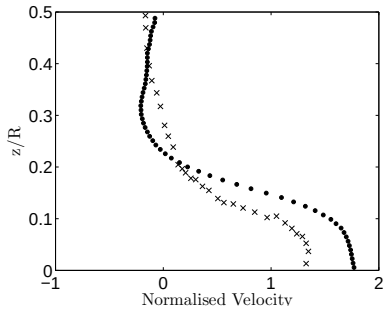

(a) $h/R = 0.5$

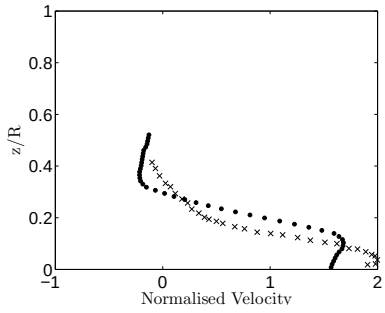

(b) $h/R = 1.0$

Figure 3: Profile of radial velocity at $r/R = 1.5$. (Crosses correspond to experimental data and dots to VTM predictions.)

Comparison of Eqs. 1 and 3 shows that the vorticity transport and particle transport equations are very similar in mathematical form. This similarity allows the particle transport equation to be run alongside the vorticity transport equation without significant increase in computational expense [7].

A sub-layer type model is used to relate the fluid velocity to the motion of the particles close to the ground plane and thus to calculate the source S_p of particulates into the flow in terms of the vertical flux of particles off the ground plane. The physics of particle transport close to the ground is very complex. Studies within the sedimentology community suggest a process in which, after a threshold velocity is reached, the largest particles start to roll and creep along the ground whilst slightly smaller particles hop in a motion called saltation. The movement of these particles disturbs the smallest particles on the ground plane, and these particles can then become suspended within the flow field. Modelling all these interactions directly is presently well beyond the state of the art. A semi-empirical model is thus used to describe this process and to relate the flow velocity along the ground plane to the amount of dust that becomes suspended in the flow. Based on the work by White [10], the horizontal particle flux, Q, is related to particle diameter and flow velocity by the expression

$$Q = Ec\upsilon^3 \frac{\rho}{g}\left(1 - \frac{\upsilon_t}{\upsilon}\right)\left(1 + \frac{\upsilon_t^2}{\upsilon^2}\right) \tag{4}$$

where E is the ratio of erodible surface to total surface area, taken here to be unity, and the empirical constant $c = 0.261$. The threshold velocity, υ_t, as described by Lu and Shao [11] is given by

$$\upsilon_t = \frac{1}{\kappa}\sqrt{a_1\left(\frac{\rho_s}{\rho}gd + \frac{a_2}{\rho d}\right)} \tag{5}$$

where the coefficients a_1 and a_2, based on wind tunnel experiments, are approximately 0.0123 and $3 \times 10^{-4}\text{kgs}^{-2}$ respectively. The presence of surface roughness elements can be accounted for by varying the constant κ, and in the simulations presented in this paper a value of 0.44 is used to represent a desert in which a distribution of rock fragments partially armour the surface [12].

Marticorena and Bergametti define the vertical particle flux as being dependent on the percentage of clay within the erodible surface [13]. The relation between the horizontal flux and the vertical flux of particulates into the air is then given by

$$S_p = Q\ e^{13.4f - 6.0} \tag{6}$$

where f is a measure of the clay content of the surface. S_p is then the particle source term in Eq. 3.

Verification of Flow Fields Produced By Rotors in Ground Effect

Prior to using the VTM to model the particle transport that is associated with brownout, it must first be shown that the VTM can predict accurately the flow field around a rotor when operating in ground effect. Previous investigations by Whitehouse and Brown [14] and Phillips and Brown [7,15] for example, have shown that the VTM is indeed capable of predicting the various distinct flow regimes encountered during low speed forward flight as described by Curtiss *et al.* [16]. It has also been shown previously that the VTM matches existing data for the variation of power with height for hovering rotors.

The ability of the VTM to predict accurately the flow field around a rotor in ground effect has been investigated further by examining the radial velocities within the wake and the trajectory of the tip vortices that are produced by the rotor blades when in ground effect. Lee *et al.* [17] conducted experiments in which digital particle image velocimetry was used to obtain velocity data from within the flow field of a rotor when hovering in ground effect. The VTM has been used to simulate the same two-bladed rotor under the same flight conditions as in this experiment. Figures 1 to 3 show an example comparison of the velocity profiles predicted by the VTM to the experimental data. Shown in the figures are the time-averaged radial velocity profiles found at three different distances ($0.8R$, $1.0R$ and $1.5R$) from the rotor axis. Each figure shows the velocity profile for the rotor hovering at two different heights ($0.5R$ and $1.0R$) above the ground. The velocities predicted using the VTM are seen to correspond well to those obtained through experiment and show clearly the formation of the radial wall jet as the wake impinges on the ground.

Flow visualisation using smoke injection was used during the experiments conducted by Lee *et al.* to highlight the structures found within the wake below the rotor. The qualitative features of the flow field predicted by the VTM are compared to one of Lee *et al.*'s images in Fig. 4. In this figure, instantaneous snapshots of the experimental and numerical flow fields both show the characteristic formation of the tip vortex and vortex sheet structures in the wake below the rotor. The numerical results (Fig. 4(b)) also reveal the onset of vortex pairing in the wake a short distance from the centre of the rotor. The associated instability of the wake is the most likely origin of the disorganised 'turbulent wall jet' that is observed experimentally at significant distances from the rotor.

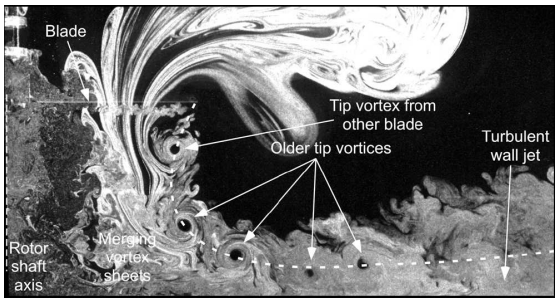

(a) Smoke flow visualisation of the wake produced by a two-bladed rotor in ground effect. Image from Lee *et al* [17]

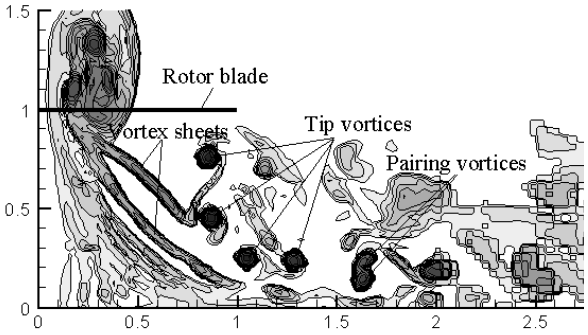

(b) Vorticity distribution from a two bladed rotor in ground effect as calculated using the VTM

Figure 4: Flow field produced by a rotor hovering at one radius above the ground as predicted by the VTM compared to that observed through experiment.

A more quantitative verification of the predictions of the VTM can be obtained by comparing VTM data for the trajectories of the tip vortices produced by the blades of a rotor in strong ground effect to the experimental data published by Light [18]. Light's experiment involved using a wide-field shadowgraph method to photograph the tip vortices of a rotor hovering at various heights above a ground board. Quantitative data regarding the positions of the vortices were then extracted from the photographs. Figures 5 and 6 compare the axial and radial positions of the tip vortices, as predicted by the VTM, to the data collected by Light. Data are presented for the rotor at three different heights above the ground. Figures 5(a) and 6(a) show the trajectories of the tip vortices when the rotor is out of ground effect, Figs. 5(b) and 6(b) show the trajectories when the rotor is at a height of $0.84R$ and Figs. 5(c) and 6(c) when the rotor is at a height of $0.52R$ above the ground. In all cases there is very good agreement between the vortex positions as predicted by the VTM and those obtained through experiment. The vortices follow a fairly steady trajectory up to a wake azimuth of approximately 200°. After this wake age the vortex positions become more scattered due to the unsteadiness within the wake that is associated with its inherent instability. The VTM is shown to capture well both the orderly development of the wake and this subsequent unsteadiness, lend-

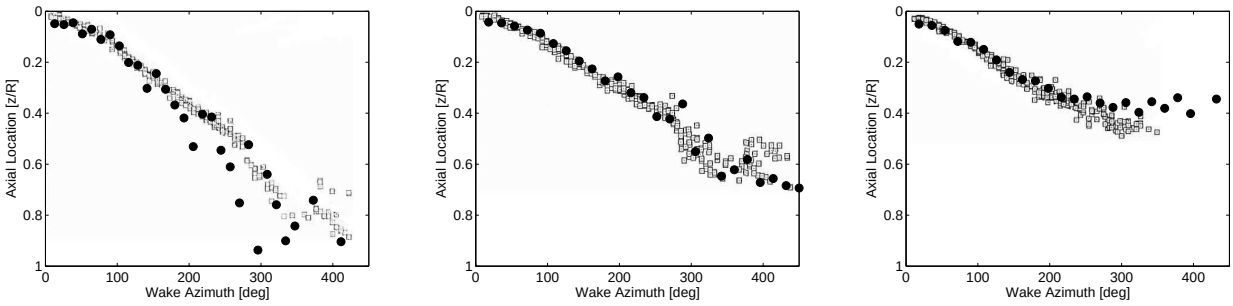

(a) Rotor hovering out of ground effect (b) Rotor hovering at a height above the ground of $0.84R$ (c) Rotor hovering at a height above the ground of $0.52R$

Figure 5: Axial locations of the tip vortices produced by a hovering rotor. (Dark circles are data predicted by the VTM, squares are experimental data of Light [18].)

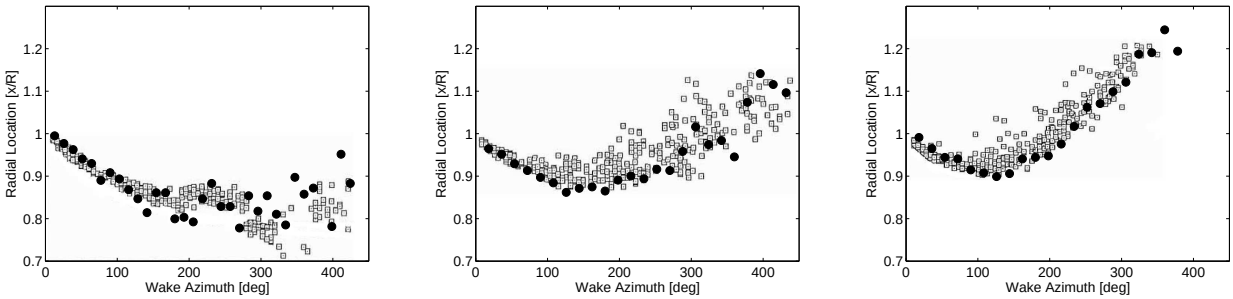

(a) Rotor hovering out of ground effect (b) Rotor hovering at a height above the ground of $0.84R$ (c) Rotor hovering at a height above the ground of $0.52R$

Figure 6: Radial locations of the tip vortices produced by a hovering rotor. (Dark circles are data predicted by the VTM, squares are experimental data of Light [18].)

ing significant confidence in the ability of the VTM to predict accurately the geometry of the wake that is produced by a helicopter rotor when it is subject to strong ground effect.

There is very limited data available that is of sufficient quality to allow direct verification of any predictions of the entrainment of dust from the ground plane into the flow surrounding the helicopter. Figures 7 and 8 show, nevertheless, a qualitative comparison between the dust distribution as predicted by the VTM and the results from a wind tunnel investigation in which talcum power was used to represent the entrainment and subsequent transport of dust particles in the flow surrounding a model rotor [8]. A sample of the vorticity distribution and the corresponding dust density distribution as predicted by the VTM is shown in Fig. 7. A comparison of these numerically generated images to the sample snapshot of the experimentally-observed dust distribution shown in Fig. 8 reveals that, qualitatively at least, the VTM reproduces the key features within the flow. Both the numerical and experimental images show the rotor tip vortices to travel along the ground plane, and, as a result of the associated local increase in velocity, a small wedge-shaped region of dust to form in front of each vortex. This comparison suggests, despite the reservations expressed earlier, that the empirical model that is used within the VTM to describe the entrainment of the particles into the flow is capable of representing faithfully the physics of the particle entrainment process that occurs during the onset and development of helicopter rotor-induced brownout.

Description of Rotor Configuration

The effect on the characteristics of the brownout phenomenon of the twist and number of the blades of the main rotor (whilst maintaining the overall solidity of the rotor) of a generic helicopter system has been investigated. A fictitious, 5-bladed rotor system was chosen as the baseline configuration about which the chosen rotor design parameter could be varied. The blades of the baseline rotor were rectangular in planform, with a NACA23012 profile along their entire span, 8° linear twist and the root cutout positioned at 25% of the blade radius. The blades were attached to an articulated rotor hub. The dimensions and operating conditions, such as rotational speed and thrust, of this generic rotor system were chosen to be representative of AgustaWestland's EH101 helicopter. The

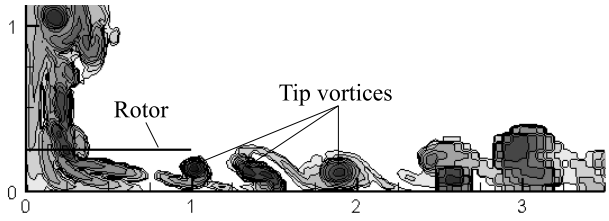

(a) Contours of vorticity distribution

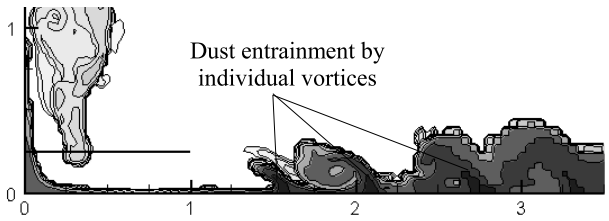

(b) Contours of dust density distribution

Figure 7: Vorticity and corresponding dust density distributions in the flow field below a rotor in ground effect as predicted using the VTM.

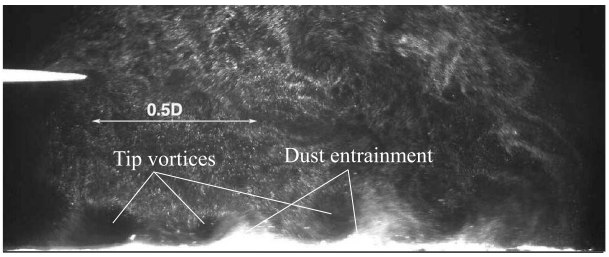

Figure 8: Snapshot showing the effect of the tip vortices on the particle distribution along the ground plane. Image from wind tunnel experiment conducted by Nathan and Green [8].

properties of the baseline rotor system are summarised in Table 1. The present study focused on the characteristics of the isolated main rotor in order to avoid obscuration of the physics by secondary effects, and hence the fuselage of the helicopter was not modelled.

Description of Overall Flow Field

Brownout is most severe when the helicopter rotor operates close to a dusty ground surface at low forward speeds. For this reason, brownout is most often encountered when landing. In the results presented in this paper, the onset of brownout during a landing manoeuvre where the helicopter approaches along the ground before decelerating into hover is approximated by separating the calculation into several intermediate stages, each simulated as an individual steady flight case. This was done to allow a fairly high-resolution representation of the flow field whilst at the same time avoiding the very high associated cost of simulating a realistic landing manoeuvre during a single computational run. While such an approach might not yield the most exact representation of a real landing manoeuvre, and some care must be taken in extrapolating the results so obtained to the real-life situation, the resulting simulations do show clearly the process through which the dust cloud is formed and evolved by the flow field that is generated by the rotor as the helicopter decelerates.

Table 1: Summary of baseline rotor properties

Rotor radius	9.3 m
Number of blades	5
Root cutout	$0.25R$
Solidity	0.124
Twist	$-8°$ (Linear)
Flap/lag hinge offset	$0.05R$
Chord	$0.078R$
Aerofoil section	NACA23012

In all the simulations presented in this paper, the centre of the rotor hub is positioned at one rotor radius above the ground. The landing approach is divided into three intermediate stages during which the helicopter is flown at thrust-normalised advance ratios $\mu^\star = 0.6$, 0.3 and 0.0. The rotor is trimmed to a constant thrust coefficient $C_T = 0.012$ and to zero disc tilt throughout[1].

The wake structures generated by the baseline rotor at each of these advance ratios are shown in Fig. 9. In this figure, representative three-dimensional snapshots of iso-contours of vorticity and dust density at each of the simulated flight conditions are shown. At $\mu^\star = 0.6$ the wake system contains a horse-shoe shaped ground vortex below the front edge of the rotor. This ground vortex entrains a large mass of dust into the flow just upstream of the rotor. The dust that is picked up in this region is transported rearwards into the flow behind the rotor where some of it is entrained into the rolled up element of the wake behind the advancing side of the rotor. Although the accumulation of dust in this part of the flow field would do little to obscure the pilot's view, it is interesting to note that the characteristic asymmetry of the roll-up of the wake on the advancing and retreating sides of the rotor produces very different shapes to the dust cloud on either side of the helicopter.

At first glance, the snapshots of dust density for $\mu^\star = 0.3$ would seem to suggest that less dust is entrained into the flow at this speed than at $\mu^\star = 0.6$. This observation is perhaps somewhat surprising since more dust might be expected to be circulated within the wake at the lower forward speed given the reduced influence of the forward speed of the helicopter com-

[1] At a thrust coefficient of $C_T = 0.012$, thrust-normalised advance ratios $\mu^\star = 0.6$ and $\mu^\star = 0.3$ correspond to advance ratios $\mu = 0.046$ and $\mu = 0.023$ respectively.

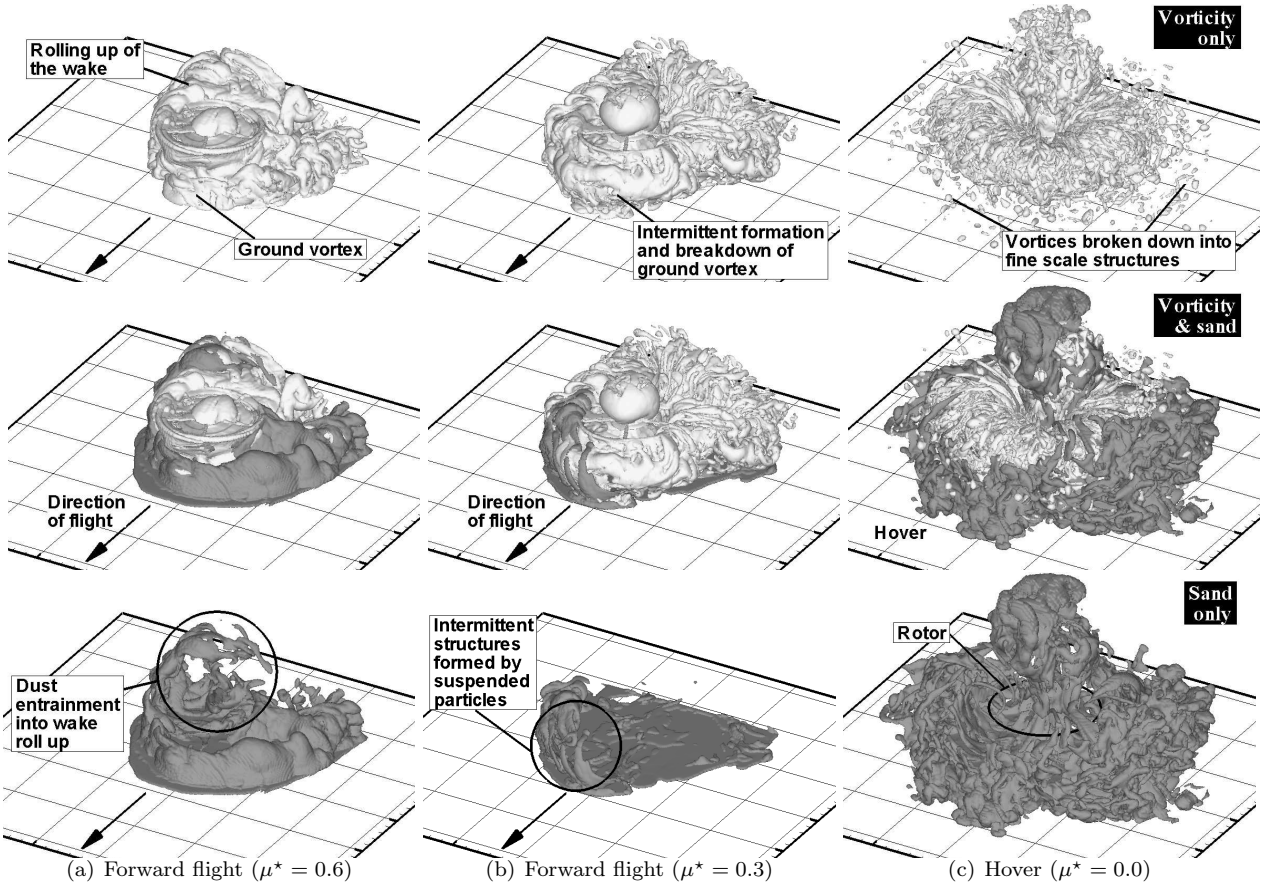

(a) Forward flight ($\mu^\star = 0.6$) (b) Forward flight ($\mu^\star = 0.3$) (c) Hover ($\mu^\star = 0.0$)

Figure 9: Instantaneous iso-contours of vorticity (light) and dust density (dark) for the baseline rotor at thrust $C_T = 0.012$. (Top: vorticity only. Centre: vorticity and sand. Bottom: sand only.)

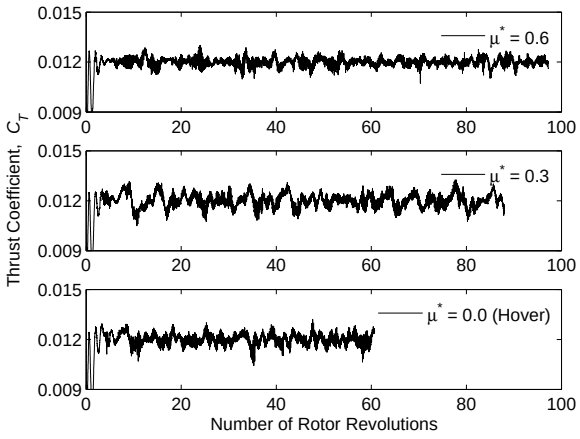

Figure 10: Time history of thrust produced by the rotor in hover and forward flight. Data lines offset for clarity.

pared to the induced flow of the rotor in convecting the dust away into the flow behind the helicopter. It should be borne in mind, however, that the iso-contours presented in Fig. 9 represent a series of instantaneous views of the flow and that the rotor flow in ground effect is highly unsteady. Figure 10 shows the time history of the thrust of the baseline rotor at the three simulated advance ratios. Of the three flight conditions presented in the figure, the time history of the thrust produced by the rotor at $\mu^\star = 0.3$ (plotted in dark grey) is seen to contain distinctive, large, low frequency fluctuations that are not as marked at the other two flight conditions. Indeed, as will be shown in the following section in more detail, the flow pattern that is produced by the rotor at this forward speed is highly intermittent, and the build-up and ejection of vorticity near the rotor occurs over relatively long time-scales compared to the other flight conditions. The effect of this unsteadiness is to produce a distribution of sand in the flow around the rotor that fluctuates markedly in density over a timescale of approximately ten to twenty rotor revolutions.

As shown in Fig. 9(c), the flow produced by the baseline rotor in hover contains a significant component of vorticity that has been disorganised into small scale features as a result of the natural instability of the wake. The extent of the disorder within the flow field appears to be a rather curious characteristic of this particular rotor and is not observed in VTM simulations of many other rotor systems. The finest scale vortices shown in the figure are the remnants of tip vortices with significant wake ages that have escaped

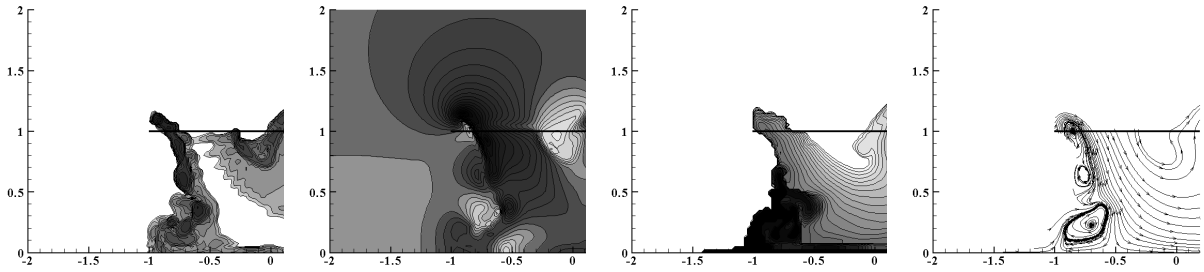

(a) Vorticity distribution (b) Velocity distribution (c) Dust distribution (d) Flow trajectories

Figure 11: Snapshot of flow field parameters around the front of the rotor disc at a thrust-normalised advance ratio $\mu^\star = 0.6$.

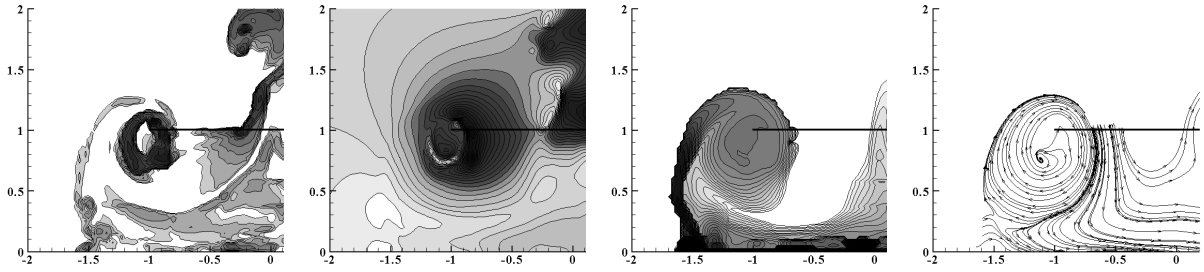

(a) Vorticity distribution (b) Velocity distribution (c) Dust distribution (d) Flow trajectories

Figure 12: Snapshot of flow field parameters around the front of the rotor disc at a thrust-normalised advance ratio $\mu^\star = 0.3$.

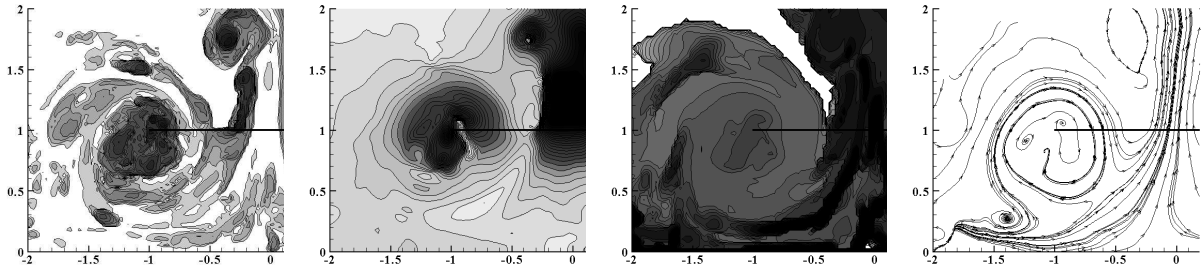

(a) Vorticity distribution (b) Velocity distribution (c) Dust distribution (d) Flow trajectories

Figure 13: Snapshot of flow field parameters around the rotor in hover.

the reach of a strongly-recirculating, toroidal flow that has its centre just outboard and below the tip of the rotor. Instead of being reingested through the rotor, these vortices remain to decompose into smaller and smaller scale structures as time progresses. The dust distribution around the rotor follows a broadly similar pattern to the vorticity, in that a part of the dust cloud that is formed is ingested through the rotor but some of the cloud appears to form sufficiently far away from the rotor that the recirculating flow has little effect on its dynamics. This yields a toroidal structure to the distribution of the recirculating sand around the edge of the rotor disc and a distinctive, wall-like structure of very high sand density further away from the rotor. Interestingly, Fig. 9(c) suggests that there may be much less sand contained in the toroidal cloud compared to in the wall-like structure. In fact, anecdotal evidence suggests that certain helicopters with similar rotor configuration to that modelled here often encounter a 'doughnut' effect while landing in dusty conditions where the flow near the rotor contains little sand to obscure the view of the pilot but forward vision is obscured a short distance away from the rotor by a significant concentration of suspended particulate matter. The computational results presented here may show evidence of such an effect.

To provide further insight into the processes that govern the entrainment of dust from the ground plane and the eventual formation of the dust clouds that are responsible for brownout, the relationship between the velocity, vorticity and dust density distributions within the flow field surrounding the rotor are next examined. Figures 11 through to 13 show the flow field produced by the baseline rotor at the three different thrust-normalised advance ratios for which data was presented previously. The plots show snapshots of

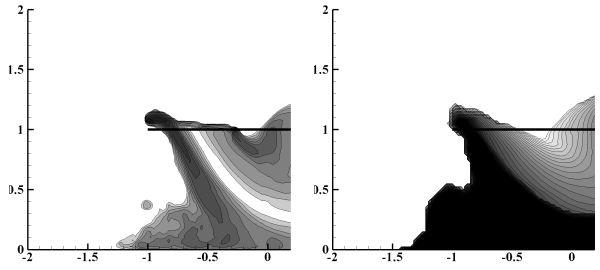

(a) Vorticity distribution (b) Dust distribution

Figure 14: Flow field parameters around the front of the rotor disc at a thrust-normalised advance ratio $\mu^\star = 0.6$. (Averaged over 20 rotor revolutions.)

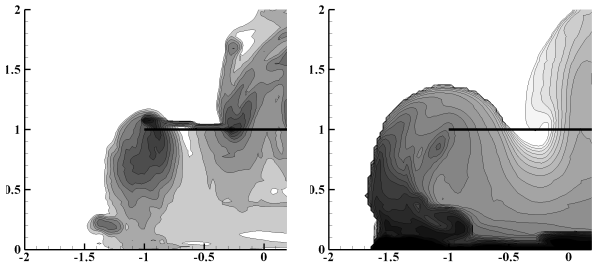

(a) Vorticity distribution (b) Dust distribution

Figure 15: Flow field parameters around the front of the rotor disc at a thrust-normalised advance ratio $\mu^\star = 0.3$. (Averaged over 20 rotor revolutions.)

the distribution of dust density, vorticity and velocity magnitude on the longitudinal plane containing the rotor axis, as well as a map of the instantaneous particle trajectories through the flow, at a representative instant of time during the simulation.

At an advance ratio of $\mu^\star = 0.6$ a persistent vortex is formed on the ground plane just below the leading edge of the rotor (Fig. 11(a)). This ground vortex remains fairly static with only minimal changes in its position and size over time — as can be inferred by comparing the snapshots of Figs. 11(a) and (c) with the plots of the averaged flow properties shown in Fig. 14. Figure 11(b) shows the largest velocities in the flow close to the ground plane to occur immediately below this vortex. Comparing the plot of velocity magnitude with that of the dust density distribution in the flow shows the initial entrainment of dust from the ground plane to occur near to the downwind edge of the ground vortex, but the dust also to remain in a thin layer close to the ground plane until around $-1R$ where the flow trajectory turns away from the ground. The highest dust density is found just upstream of a strong recirculation of particles that is centred on the ground vortex.

The structure of the wake becomes less regular at lower advance ratio. Figure 12 shows equivalent images to those in Fig. 11 but for a forward speed of the baseline rotor of $\mu^\star = 0.3$. At the particular instant in time that is represented by the figure, the wake recirculates through the leading edge of the rotor rather than forming a ground vortex as was the case at the higher advance ratio. This recirculation is intermittent, however, and breaks down on occasion to form a much more irregular flow. Separation of the flow from the ground plane generally takes place at around $-1.5R$ and it is at this point that the majority of the dust is transported out of the entrainment layer near to the ground either to be trapped in the recirculation zone located near the front of the rotor or eventually to be transported into the flow downstream of the system.

A significant difference between the instantaneous and average flow fields is revealed when the snapshots shown in Fig. 12 are compared to the long-term averages of the dust density and vorticity distributions within the flow shown in Fig. 15. This is evidence of the highly unsteady nature of the flow field produced by the rotor at this forward speed. The unsteadiness of the flow field and the associated dust cloud at $\mu^\star = 0.3$ is captured in the sequence of snapshots presented in Fig. 16. These images reveal a process through which the vorticity builds up around the rotor ($t = 49.2$ to 56.7 revs), subsequently to be ejected towards the ground ($t = 57.8$ revs). The ejected vorticity approaches the ground to form, at least momentarily, a ground vortex that acts to entrain a mass of dust below the front of the rotor ($t = 59.6$ to 62.5 revs). The ground vortex penetrates some distance upstream of the rotor only to break down into a number of smaller structures ($t = 63.0$ revs) which are then either swept downstream or reingested through the rotor. The repetition of this process over time results in the accumulation of a large but relatively amorphous cloud of particulate matter in the air surrounding the rotor.

Figure 13 shows the regime of established outwards flow below the rotor when in hover to extend only marginally further outboard of the rotor than when in low-speed forward flight at $\mu^\star = 0.3$. The similarity between the snapshots of the vorticity and dust density distributions and their averages shown in Fig. 18 (c) suggests however that the flow-field that is produced by the hovering rotor is far more constant than that produced by the rotor at $\mu^\star = 0.3$. The result is a dust cloud that is significantly greater in both size and density than in low-speed forward flight. With the rotor in hover, some of the entrained dust is trapped in the toroidal recirculatory flow just below the rotor disc, but a significant proportion escapes the recirculation to rise in a plume through the centre of the rotor. Indeed, the instantaneous image shows the greatest dust densities to occur close to the ground plane and within the plume of dust above the centre of the rotor. Conversely, the lowest dust densities are found in the recirculatory region around the edge of the rotor disc.

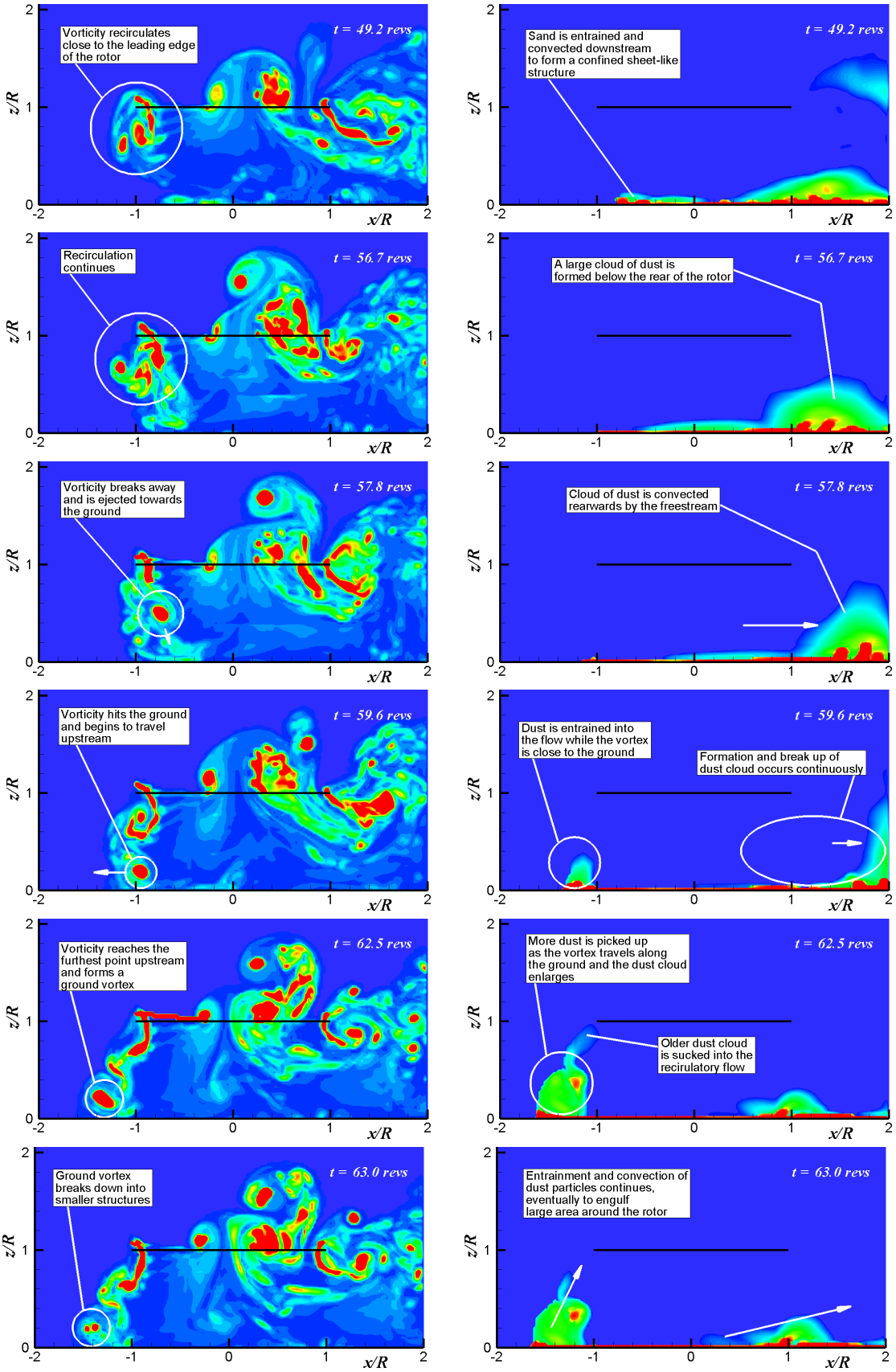

Figure 16: A sequence of sectional snapshots through the centre of the rotor in forward flight at thrust-normalised advance ratio $\mu^\star = 0.3$ at thrust $C_T = 0.012$. (Left: vorticity. Right: sand density. Red: highest contour value. Blue: lowest contour value.)

Influence of Rotor Design

The formation and subsequent evolution of the dust cloud in brownout is intimately related to the velocity field that is generated by the rotor. While the mean downwash is dictated by the disc loading of the rotor, the detailed characteristics of the induced flow field are known to be influenced by the design of the rotor. The aim of this section of the paper is to explore the sensitivity of the shape and size of the brownout cloud to two of the rotor geometric characteristics, namely the number of rotor blades and their twist. The hope is that if the relationship between rotor geometry and the resultant characteristics of the brownout cloud can be understood, then the brownout problem might eventually be mitigated simply through appropriate aerodynamic design of the rotor.

Dust particles become airborne under the action of the induced velocity produced by the rotor. More specifically, the impingement of the wake on the ground plays a key role in initiating the entrainment of the dust particles from the ground into the flow surrounding the helicopter. As shown in the previous section of this paper, the interaction of the tip vortices with the ground is by far the strongest contributor to the initial development of the dust cloud. Whilst vortex-momentum theory [19] shows that the total circulation, or, equivalently, vorticity, that is released from the rotor will be the same for a given thrust and disc area no matter what the design of the rotor, the *distribution* of vorticity from the rotor as it impinges on the ground can be modified by changing the design of the rotor. Since the vorticity originates on the blades of the rotor, the distribution of vorticity that is ejected into the flow can be altered by changing the design of the blades (e.g. their twist) or the number of blades on the rotor (while keeping constant the overall solidity of the rotor). The link between rotor design and the properties of the resulting dust cloud, as mediated by the detailed vorticity distribution that is released onto the ground, has thus been investigated by simulating the evolution of the dust cloud that is produced by four different rotor systems, each identical to the baseline rotor used in the previous section of the paper except for the number of blades. The four rotor systems that were simulated had 3, 4, 5, and 7 blades respectively. In all cases, the overall solidity of the rotor was maintained by adjusting the chord of the blades appropriately. Each rotor thus produces a different distribution of vorticity on the ground plane by generating a different number of coherent tip vortices with different spacing.

A previous study by Phillips and Brown [15] has suggested that the dust cloud produced by a rotor system with a smaller blade twist might produce a denser dust cloud than that produced by a similar system with a higher twist. Although this earlier study was rather tentative, the results suggested a link between the amount of particulate matter that is entrained into the flow field and the fairly subtle features of the distribution of downwash (or, equivalently, the vorticity distribution in the wake) that is produced below the rotor. In this paper, the effect of blade twist on the development of the dust cloud is investigated more systematically than in the previous study by comparing the behaviour of the baseline rotor in slow-speed forward flight as well as in hover to the behaviour of the rotor when modified to have four different amounts of blade twist (8°, 11°, 13° and 16°).

Effect of Number of Blades on Brownout

The effect of altering the number of rotor blades on the dust density distribution in the flow around the rotor can be inferred from Figs. 17, 18 and 19. These figures show the average over twenty rotor revolutions of the dust and vorticity distribution around the rotor in slow-speed forward flight and hover and suggest that the density of the resulting dust cloud is reduced when the circulation is distributed over a larger number of blades.

At the highest forward speed that was simulated ($\mu^\star = 0.6$, Fig. 17), changing the number of blades on the rotor appears to have little effect on the characteristics of the resultant dust cloud. This observation is perhaps unsurprising though since the interaction between the wake of the rotor and the ground is weaker the higher the forward speed of the rotor.

At $\mu^\star = 0.3$, however, the effect of changing the number of blades is clearly evident. At this advance ratio, for all four rotor configurations, the geometry and extent of the dust cloud formed around the front of the rotor is very similar, but, as the number of blades is increased, the density of dust within the cloud reduces significantly. As the number of blades is increased a greater number of tip vortices is obviously produced but the strength of each individual vortex is reduced. It appears that this reduction in strength, and the inherently non-linear relationship between the velocity that is induced on the ground plane and the amount of dust that is entrained locally as a result, conspire to reduce the amount of dust that is picked up by each individual tip vortex as it interacts with the ground plane. Overall, this effect results in less dust being present in the flow field surrounding a rotor with a comparatively larger number of blades.

Figure 19 again shows clearly the impact of the distribution of circulation on the extent of the dust cloud formed in the vicinity of the hovering rotor. The simulations of the development of the dust cloud produced by the various rotors in hover reveal a large, high density cloud of particulate matter to extend approximately two rotor radii beyond the edge of the rotor. In hover, the strength of the tip vortices is inversely pro-

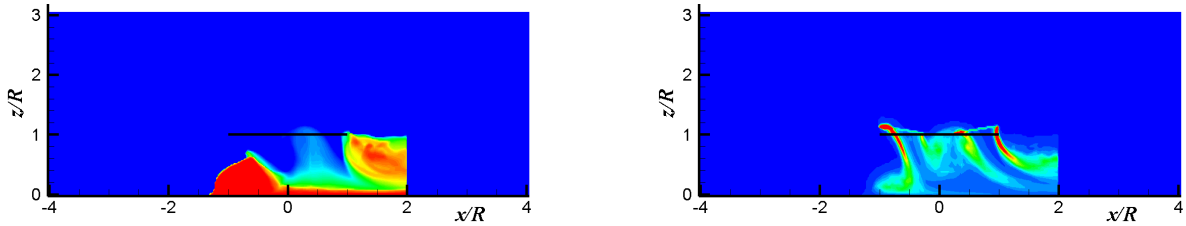

(a) 3-bladed rotor

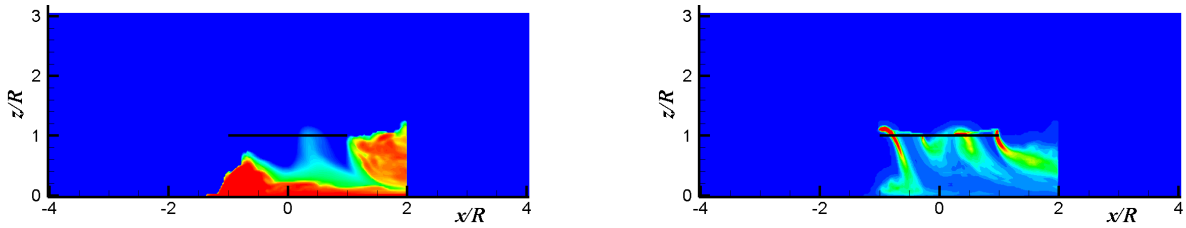

(b) 4-bladed rotor

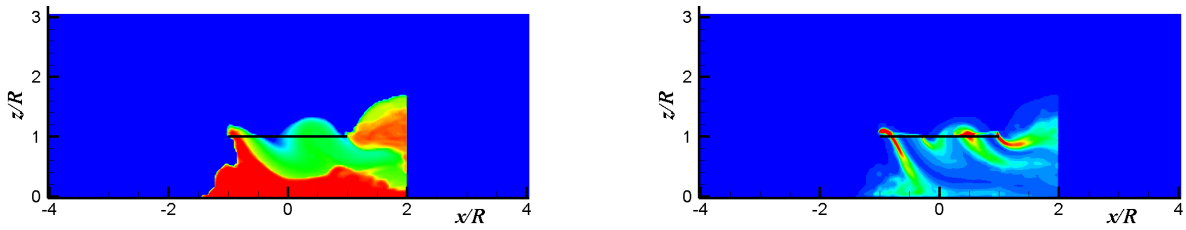

(c) 5-bladed rotor

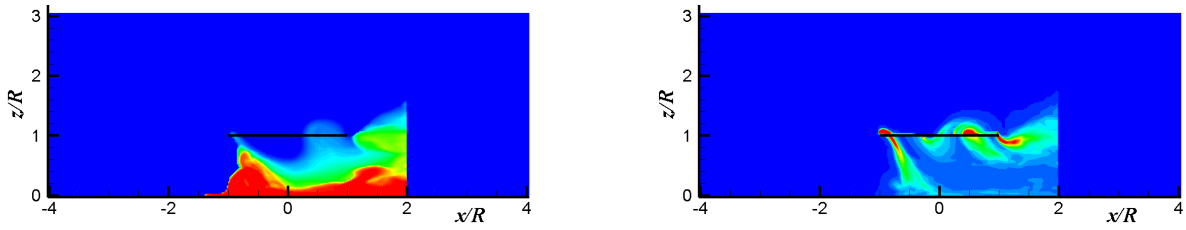

(d) 7-bladed rotor

Figure 17: Distributions of dust density (left) and vorticity magnitude (right) on vertical plane through the centre of the rotor hub in slow-speed forward flight. Thrust-normalised advance ratio, $\mu^\star = 0.6$. (Averaged over 20 rotor revolutions. Red: highest contour value. Blue: lowest contour value.)

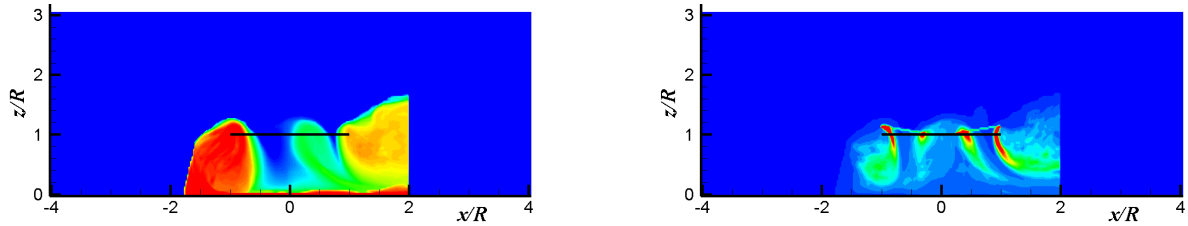

(a) 3-bladed rotor

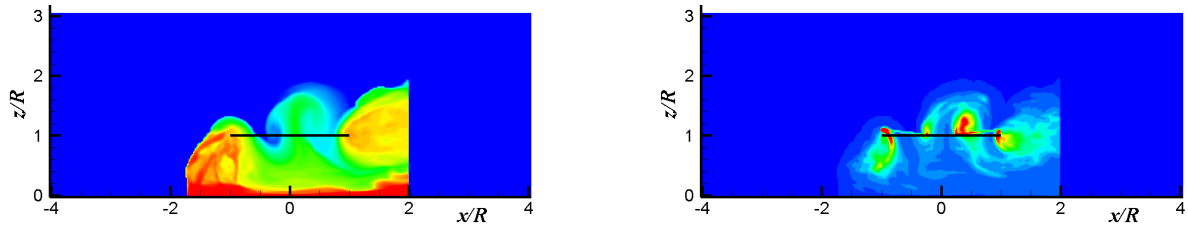

(b) 4-bladed rotor

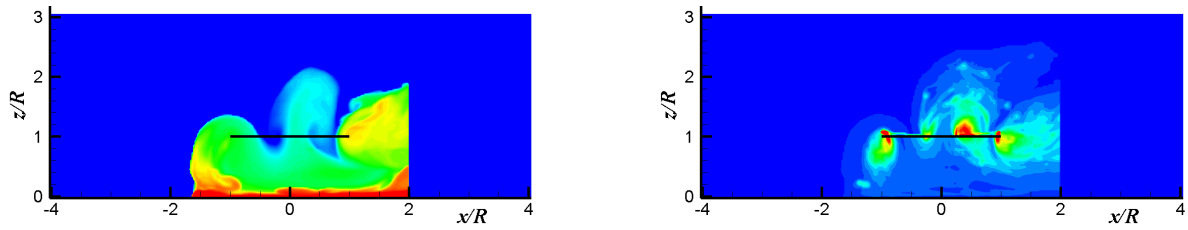

(c) 5-bladed rotor

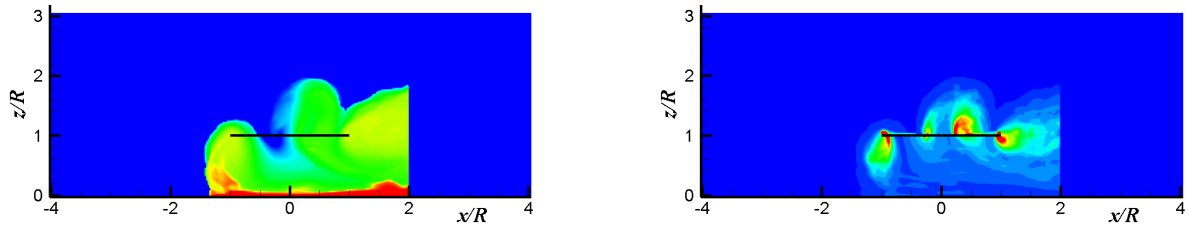

(d) 7-bladed rotor

Figure 18: Distributions of dust density (left) and vorticity magnitude (right) on vertical plane through the centre of the rotor hub in slow-speed forward flight. Thrust-normalised advance ratio, $\mu^\star = 0.3$. (Averaged over 20 rotor revolutions. Red: highest contour value. Blue: lowest contour value.)

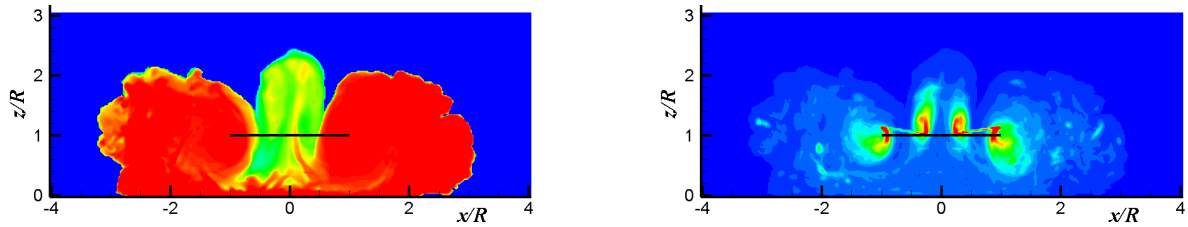

(a) 3-bladed rotor

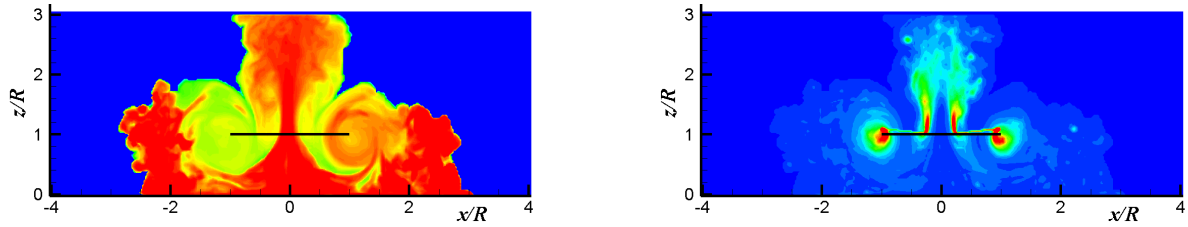

(b) 4-bladed rotor

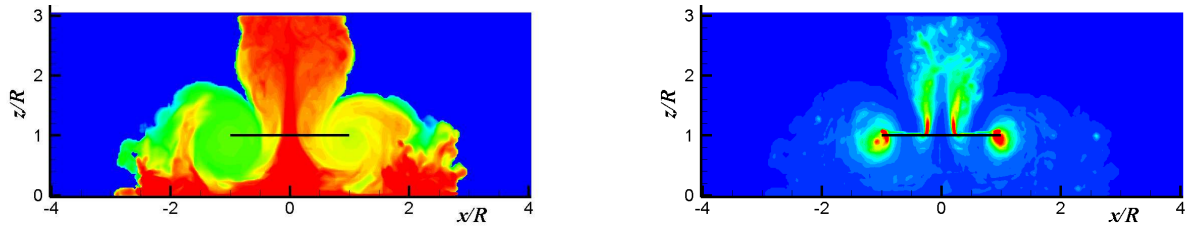

(c) 5-bladed rotor

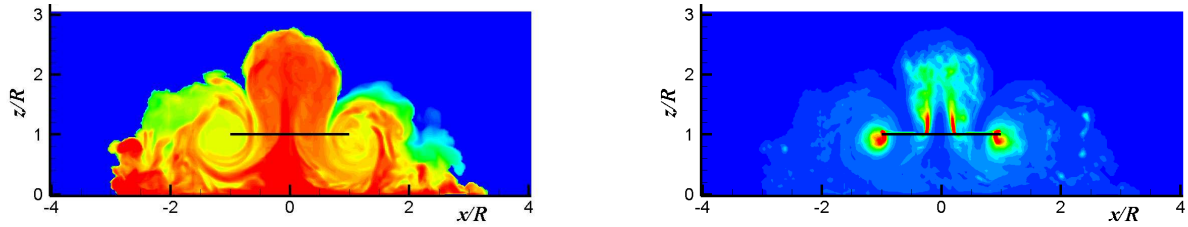

(d) 7-bladed rotor

Figure 19: Distributions of dust density (left) and vorticity magnitude (right) on vertical plane through the centre of the rotor hub in hover. (Averaged over 20 rotor revolutions. Red: highest contour value. Blue: lowest contour value.)

portional to the number of blades, and hence is greatest for the 3-bladed rotor. As the number of blades is increased from three to four, five, and eventually seven (recalling that the blade chord is adjusted accordingly to maintain the overall solidity of the rotor) a marked reduction in the dust density is evident at the core of the toroidal dust cloud that is located near the edge of the rotor disc. Conversely, more dust appears to be entrained into the plume that is convected upwards through the centre of the rotor. The extent of this dust plume correlates well with the corresponding plots of the vorticity distribution in the flow, shown on the right-hand side of the figure. It is worth cautioning, however, that the characteristics of the dust plume may be modified significantly in the real world by the presence of the helicopter fuselage.

More interesting perhaps is the behaviour of the region of high dust density just above the ground plane at a distance of approximately two rotor radii away from the centre of the rotor. The 3-bladed rotor generates a cloud of relatively high but uniform density throughout, and the wall-like feature observed in the dust distribution produced by the baseline rotor with five blades is not clearly apparent. In contrast, as the number of blades is increased, the density of the dust field is seen to become considerably more non-uniform. Indeed, the rotors with four, five and seven blades all produce a wall-like structure with high dust density at approximately two rotor radii away from the centre of the rotor. The density of the dust in this structure reduces considerably, nevertheless, as the number of rotor blades is increased.

Effect of Blade Twist on Brownout

The effect of blade twist on the geometry and density of the dust cloud produced during slow-speed forward flight is shown in Figs. 20 through to 22. At the highest advance ratio that was simulated, ($\mu^\star = 0.6$, Fig. 20), the rotor with most highly-twisted blades (16°) is seen to generate a dust cloud that has the minimum potential of all the systems simulated to obscure the view of the pilot. In this case the entire dust cloud is confined close to the ground. The rotors with less twisted blades all produce a dust cloud that engulfs the entire space between the rotor and the ground plane.

Figure 21 raises the interesting possibility that the intensity of the dust cloud that is produced by the rotor at very low advance ratios may bear a non-linear relationship to the twist of the blades. The blades with 11° of linear twist (shown in Fig. 21(b)) produce a dust cloud that is smaller in size and lower in density than the clouds produced by blades with both higher and lower twist. In all four cases that were simulated, the dust is seen to recirculate through the leading edge of the rotor. The rotor with 11° of blade twist appears to generate a much lower density of dust in this recirculation than any of the other rotors that were simulated, and, indeed, the highest dust densities produced by this rotor are encountered in the immediate vicinity of the ground plane itself rather than in the recirculating cloud near the leading edge of the rotor. Conversely, the highest dust densities within the recirculating cloud of dust are produced by the blades with 16° of twist.

As shown in Fig. 22, when the rotor is hovering above the ground plane, the most prominent difference between the dust clouds generated by the rotors with different blade twist appears to be in the extent of the plume of dust that is ejected upward through the centre of the rotor. Reducing the blade twist produces a larger and denser plume of dust above the rotor. This is most likely a consequence of the associated increase in the induced downwash close to the centre of the rotor which acts to prevent dust and vorticity from escaping vertically away through the centre of the rotor as the blade twist is increased. As well as a decrease in the height to which the dust plume reaches, there is also a significant decrease in the density of the dust within this region as the twist of the blades is increased.

The character of the dust cloud in hover appears to bear the same non-linear relationship to the twist of the rotor blades as in low-speed forward flight. Indeed, an accumulation of dust is seen to form at around two radii from the centre of the rotor in all cases, but the vertical extent above the ground of this feature of the dust distribution seems to be the smallest when the blades have 11° of twist.

Further examination of Figs. 22(c) and (d) reveals that the distribution of dust density, when averaged over twenty rotor revolutions, is far more asymmetrical than the corresponding vorticity distribution. This suggests the existence of rather disparate timescales for the evolution of the dust field and the rotor wake. A more detailed examination of the flow field shows the denser cloud of dust on the left-hand side of Fig. 22(c) and on the right-hand side of Fig. 22(d)) to result from an intermittency in the recirculatory flow pattern near the tip of the rotor that allows it on occasion to expand asymmetrically to the extent that it is capable of capturing already-suspended particles from the plume of dust above the centre of the rotor. This entrainment mechanism is illustrated in Fig. 23, and is responsible for a series of temporary, but relatively long-lived, asymmetries in the dust distribution within the recirculatory flow near the tip of the rotor. Although one might assume the dust cloud produced by a hovering rotor to be fairly steady and perhaps symmetrical, this is evidently not the case due to the process described above. It should be borne in mind however that the dust cloud that is formed above the rotor in the present simulations may be unrealistically large and dense given that the fuselage was not present, and

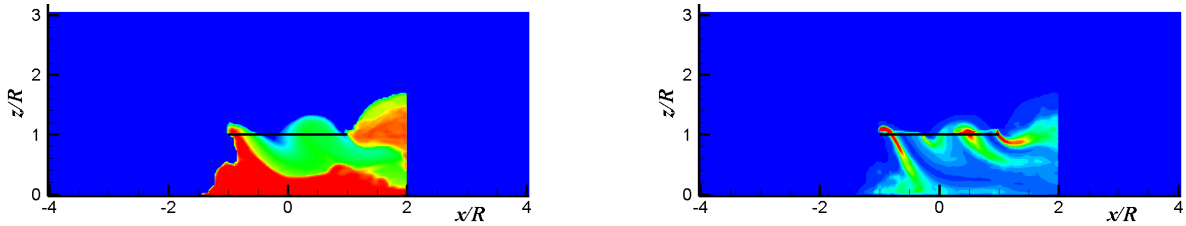

(a) Total twist $\theta_{tw} = -8°$

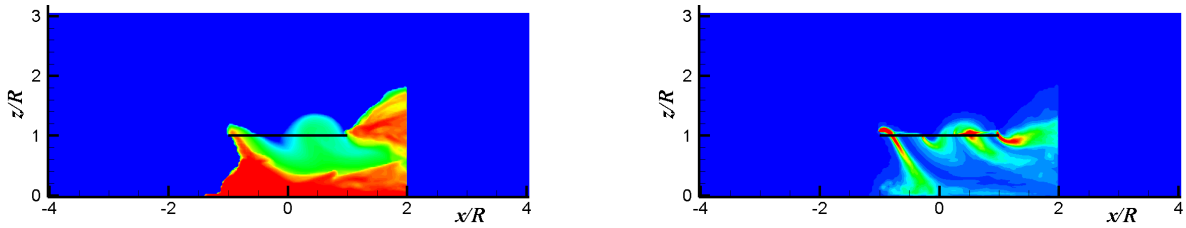

(b) Total twist $\theta_{tw} = -11°$

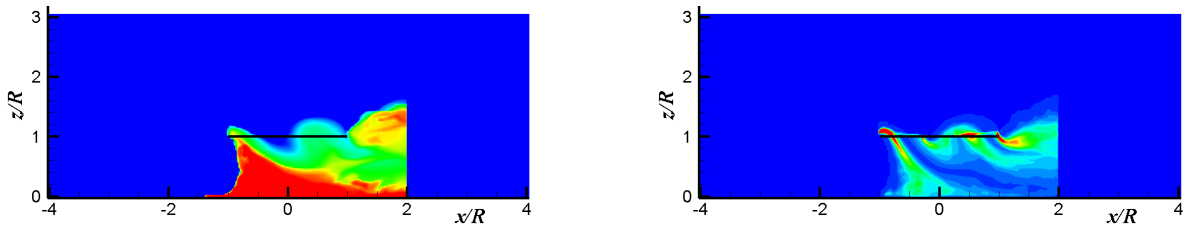

(c) Total twist $\theta_{tw} = -13°$

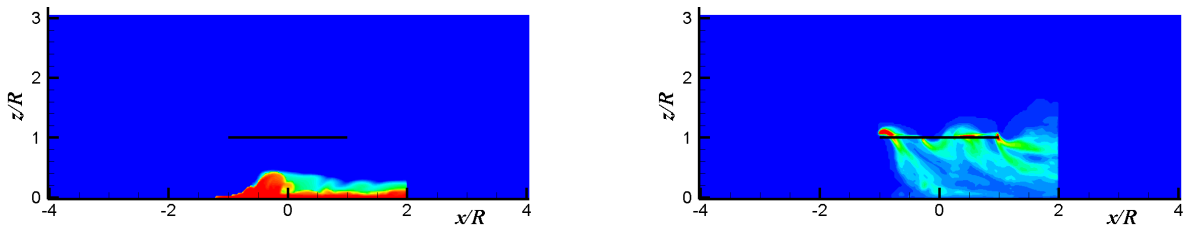

(d) Total twist $\theta_{tw} = -16°$

Figure 20: Distributions of dust density (left) and vorticity magnitude (right) on vertical plane through the centre of the rotor hub in slow-speed forward flight. Thrust-normalised advance ratio, $\mu^\star = 0.6$. (Averaged over 20 rotor revolutions. Red: highest contour value. Blue: lowest contour value.)

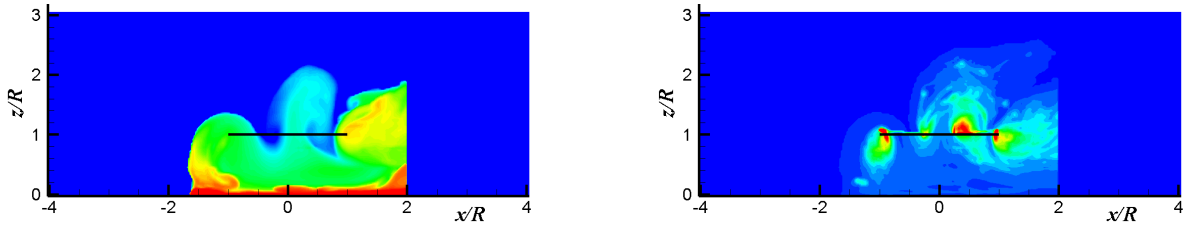

(a) Total twist $\theta_{tw} = -8°$

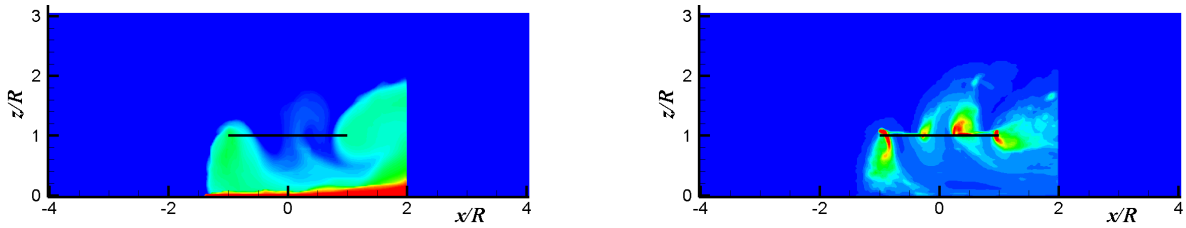

(b) Total twist $\theta_{tw} = -11°$

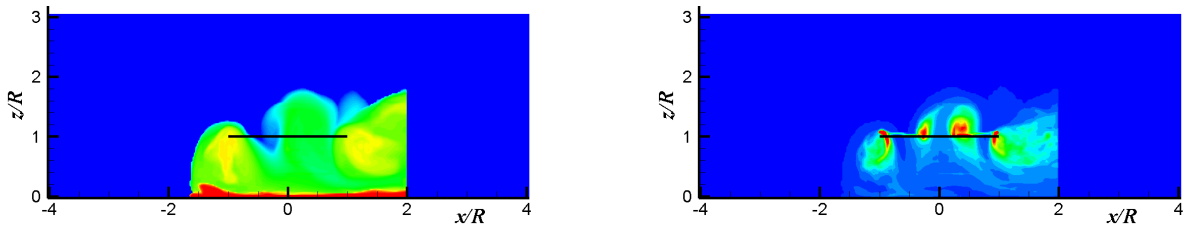

(c) Total twist $\theta_{tw} = -13°$

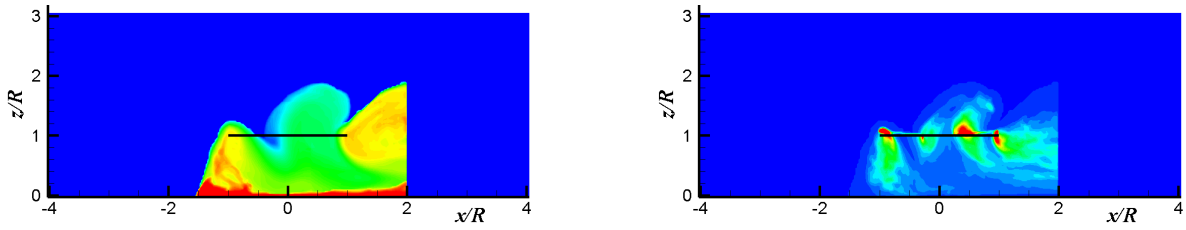

(d) Total twist $\theta_{tw} = -16°$

Figure 21: Distributions of dust density (left) and vorticity magnitude (right) on vertical plane through the centre of the rotor hub in slow-speed forward flight. Thrust-normalised advance ratio, $\mu^\star = 0.3$. (Averaged over 20 rotor revolutions. Red: highest contour value. Blue: lowest contour value.)

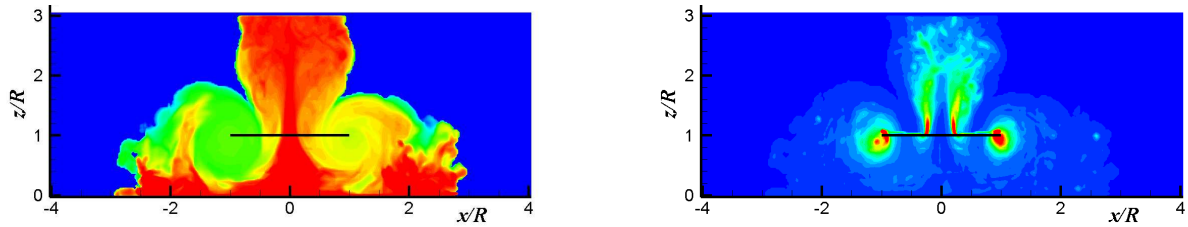

(a) Total twist $\theta_{tw} = -8°$

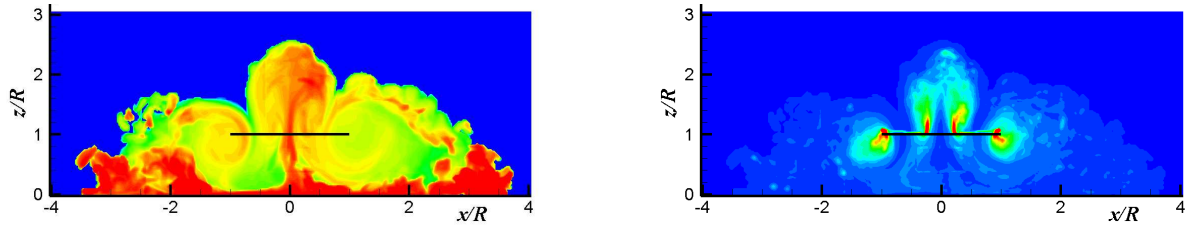

(b) Total twist $\theta_{tw} = -11°$

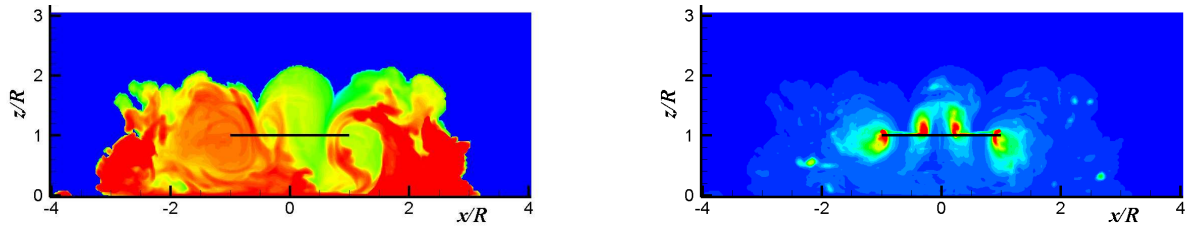

(c) Total twist $\theta_{tw} = -13°$

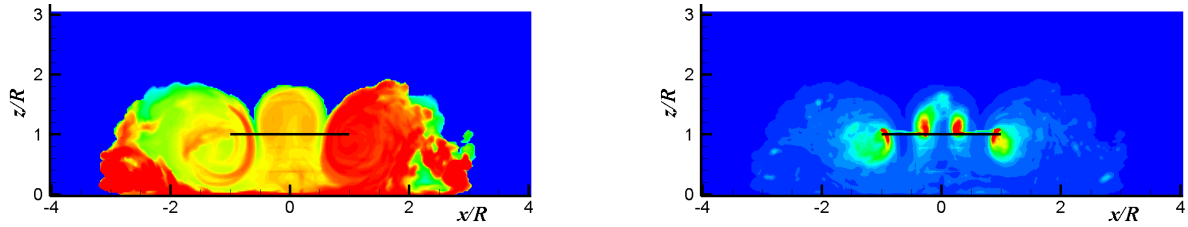

(d) Total twist $\theta_{tw} = -16°$

Figure 22: Distributions of dust density (left) and vorticity magnitude (right) on vertical plane through the centre of the rotor hub in hover. (Averaged over 20 rotor revolutions. Red: highest contour value. Blue: lowest contour value.)

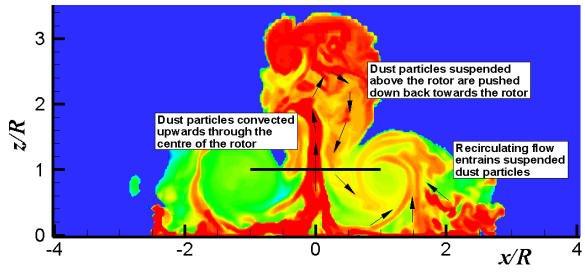

Figure 23: A sectional snapshot through the dust cloud that is generated by the rotor in hover ($C_T = 0.012$. Red: highest contour value. Blue: lowest contour value.)

hence that the resulting asymmetries in the simulated dust cloud might be somewhat larger than observed in practice. Nevertheless, the observations presented here suggest crucially that the long-term characteristics of the dust cloud that is produced under brownout conditions are dependent not only on the mean properties of the flow-field that is produced by the rotor but also on the continuous interaction between the forming cloud and the unsteadiness in the flow field that is characteristically produced by all helicopter rotors when operating in strong ground effect. This raises the bar considerably in terms of the fidelity of the representation of the rotor wake that is required to capture accurately the onset and development of rotor-induced brownout.

Conclusions

The Vorticity Transport model, augmented with an additional equation to model the transport of particles within the flow, has been used to simulate the development of the dust clouds that can form around helicopters while performing landing manoeuvres in desert or dusty environments. The dust clouds that develop can obscure the pilot's view resulting in a potentially dangerous situation known as brownout. Anecdotal evidence suggests that different types of helicopters have very different brownout characteristics. It is thought that some of the geometric characteristics of the rotor might thus play an important role in determining the size and density of the dust clouds that are produced by any particular type of helicopter.

The Vorticity Transport Model has been used to investigate the sensitivity of the characteristics of the brownout cloud to the number of blades of the main rotor and to their twist. The VTM has been shown to predict accurately the characteristics of the flow field around a rotor operating in ground effect. The entrainment of dust from the ground plane into the flow field surrounding the helicopter is related to the velocity distribution within the wake, and the VTM has been shown to predict well the variation of outwash velocity both with height above the ground as well as distance from the rotor. Of critical importance to the difference in the development of the dust clouds that are generated by different rotors appears to be the dynamics of the individual tip vortices as they interact with the ground. Indeed, qualitative results have been presented that show how each individual vortex is responsible for entraining particles from the ground plane into the flow. The VTM has been shown to predict the position of these vortices accurately as they interact with the ground.

Simulations of the onset and development of brownout have been conducted using a five-bladed rotor with 8° of linear twist as a baseline model. Simulations at three different advance ratios were conducted to represent a helicopter coming in to land. Instantaneous snapshots of the flow field surrounding the rotor at each advance ratio show the structure of the wake to be highly dependent on forward speed. At the fastest advance ratio a fairly constant ground vortex forms below the rotor and entrains a significant amount of dust. Most of this dust remains close to the ground, however, where it does not interfere with pilot visibility. As the forward speed of the helicopter is reduced, the wake becomes more unsteady and recirculates around the leading edge of the rotor disc. A concentration of vorticity builds up around the rotor before being ejected towards the ground. As this vorticity interacts with the ground, particles are picked up and are then transported within the flow around the rotor. When the rotor is in hover, a much larger cloud of recirculating dust forms in a toroid around the rotor.

The number of blades, thus the number and strength of the tip vortices, and also the twist of the blades is thought to have an effect on the size, shape and density of the dust clouds that accumulate around the helicopter under brownout conditions. To investigate the effect of these two geometric characteristics of the rotor on the formation of brownout, the number of blades and blade twist of the baseline rotor were altered while keeping the rotor solidity constant throughout. It was found that the number of blades of the rotor has a significant effect on the density of the dust within the clouds. As the number of blades is increased, the density of dust around the rotor decreases as the total circulation released from the rotor is distributed among a greater number of tip vortices. This was found to be the case at all advance ratios that were simulated. Altering the twist of the blades does not appear to produce such a linear outcome. Of the values of twist that were investigated, a twist of 11° resulted in the dust cloud with the lowest density; rotors with lower or higher twist appear to produce denser dust clouds under the same operating conditions.

The results presented in this paper lend insight into the development and evolution of the dust cloud that forms when a rotor wake interacts with a dusty surface.

The results show that the geometric characteristics of the main rotor can have a significant effect on the size and density of the dust cloud that is produced under brownout conditions, and thus that passive aerodynamic measures may well be considered as a possible means for ameliorating the effects of brownout on helicopter operations.

References

[1]Keller, J.D., Whitehouse, G.R., Wachspress, D.A., Teske, M.E., and Quackenbush, T.R., "A Physics-Based Model of Rotorcraft Brownout for Flight Simulation Applications," 62nd Annual Forum of the American Helicopter Society, Phoenix, AZ, 9–11 May 2006.

[2]Whitehouse, G.R., Wachspress, D.A., Quackenbush, T.R., and Keller, J.D., "Exploring Aerodynamic Methods for Mitigating Brownout," 65th Annual Forum of the American Helicopter Society, Grapevine, TX, 27–29 May 2009.

[3]Ryerson, C.C., Haehnel, R.B., Koenig, G.G., and Moulton, M.A., "Visibility Enhancement in Rotorwash Clouds," 43rd AIAA Aerospace Sciences Meeting and Exhibit, Reno, NV, 10-13 January 2005.

[4]Haehnel, R.B., Moulton, M.A., Wenren, Y., and Steinhoff, J., "A Model to Simulate Rotorcraft-Induced Brownout," 64th Annual Forum of the American Helicopter Society, Montréal, Canada, 29 April–1 May 2008.

[5]Brown, R.E., "Rotor Wake Modeling for Flight Dynamic Simulation of Helicopters," *AIAA Journal*, Vol. 38 (1), January 2000, pp. 57–63.

[6]Brown, R.E. and Line, A.J., "Efficient High-Resolution Wake Modeling Using the Vorticity Transport Equation," *AIAA Journal*, Vol. 43 (7), July 2005, pp. 1434–1443.

[7]Phillips, C. and Brown, R.E., "Eulerian Simulation of the Fluid Dynamics of Helicopter Brownout," 64th Annual Forum of the American Helicopter Society, Montréal, Canada, 29 April–1 May 2008.

[8]Nathan, N.D. and Green, R.B., "Measurements of a Rotor Flow in Ground Effect and Visualisation of the Brown-out Phenomonon," 64th Annual Forum of the American Helicopter Society, Montréal, Canada, 29 April–1 May 2008.

[9]Johnson, B., Leishman, J.G., and Sydney, A., "Investigation of Sediment Entrainment in Brownout Using High-Speed Particle Image Velocimetry," 65th Annual Forum of the American Helicopter Society, Grapevine, TX, 27–29 May 2009.

[10]White, B. R., "Soil Transport by Winds on Mars," *Journal of Geophysical Research*, Vol. 84 (B9), August 1979, pp. 4643–4651.

[11]Lu, H. and Shao, Y., "Toward Quantitative Prediction of Dust Storms: An Integrated Wind Erosion Modelling System and its Applications," *Environmental Modelling and Software*, Vol. 16 (3), April 2001, pp. 233–249.

[12]MacKinnon, D.J., Clow, G.D., Tigges, R.K., Reynolds, R.L., and Chavez, P.S. Jr., "Comparison of Aerodynamically and Model-derived Roughness Lengths (Zo) Over Diverse Surfaces, Central Mojave Desert, California, USA," *Geomorphology*, Vol. 63 (1-2), November 2004, pp. 103–113.

[13]Marticorena, B. and Bergametti, G., "Modeling the Atmospheric Dust Cycle: 1. Design of a soil-derived dust emission scheme," *Journal of Geophysical Research*, Vol. 100 (D8), August 1995, pp. 16415–16430.

[14]Whitehouse, G.R. and Brown, R.E., "Modelling Rotor Wakes in Ground Effect," *Journal of the American Helicopter Society*, Vol. 49 (3), July 2004, pp. 238–249.

[15]Phillips, C. and Brown, R.E., "The Effect of Helicopter Configuration on the Fluid Dynamics of Brownout," 34th European Rotorcraft Forum, Liverpool, UK, 16–19 September 2008.

[16]Curtiss, H.C. Jr., Erdman, W., and Sun, M., "Ground Effect Aerodynamics," *Vertica*, Vol. 11 (1-2), 1987, pp. 29–42.

[17]Lee, T.E., Leishman, J.G., and Ramasamy, M., "Fluid Dynamics of Interacting Blade Tip Vortices With a Ground Plane," 64th Annual Forum of the American Helicopter Society, Montréal, Canada, 29 April–1 May 2008.

[18]Light, J.S., "Tip Vortex Geometry of a Hovering Helicopter Rotor in Ground Effect," *Journal of the American Helicopter Society*, Vol. 38 (2), April 1993, pp. 34–42.

[19]Stepniewski, W.Z. and Keys, C.N., *Rotary-Wing Aerodynamics*, Dover Publications, 1984.